J. Fluid Mech. (1994), *vol.* 264, *pp.* 277–301

Dynamics of an isolated barotropic eddy on a beta-plane

By GENNADY K. KOROTAEV AND ALEXANDER B. FEDOTOV
Marine Hydrophysical Institute, Sevastopol 335000 Ukraine

(Received 29 November 1992 and in revised form 12 July 1993)

The dynamics of a Gaussian isolated barotropic eddy on a β-plane is considered. The analytical solution of the evolution of an isolated vortex is constructed by analogy to the theory of a point vortex. The results of a numerical experiment are compared with the conclusions of the theory for the case of the Gaussian vortex. Characteristics of the vortex such as its radius, trajectory of movement, kinetic energy, residual vorticity, and the structure of the vortex are discussed. The analysis of the numerical results shows that the experimentally determined radius of the vortex, its energy, and residual vorticity are in good agreement with the theory. On the other hand there is a difference between analytical and experimental values of velocity components, and hence in the trajectory of the centre of the vortex. The location of the separatrix of the streak function and its saddle point are considered as important characteristics of the structure of the vortex. We consider the phenomenon of the generation of the vortex sheet connected with the separatrix location as a cause of the difference between the experimental and analytical estimates of the velocity of the vortex.

1. Introduction

The problem of the evolution of an isolated vortex on a β-plane has been intensively investigated for more than forty years. The interest in this problem is especially strong in meteorology, namely concerning tropical cyclone movement. Oceanographers also became interested in the dynamics of intensive eddies after the large-scale oceanographic experiments POLYGON-70, MODE and POLYMODE, where cyclone and anticyclone types of eddies were observed. As a result, numerous analytical and numerical studies of isolated eddy dynamics were carried out (Adem 1956; Bretherton & Karweit, 1975; McWilliams & Flierl 1979; Flierl 1984; Shapiro & Ooyama 1989; Cushman-Roisin, Chassignet & Tang 1990; Smith & Ulrich 1990; Smith, Ulrich & Dietachmayer 1990). In spite of all these attempts, the physics of eddy evolution are still far from completely understood.

A speculative analytical model similar to that of Flierl (1984) was elaborated by one of the present authors (Korotaev 1980*a*, *b*, 1988) for the case of a point barotropic vortex. This model has a very clear physical meaning but it is based on some assumptions which do not have strict foundations. The present work is a further development of this model for the case of a continuous initial vorticity distribution, and tests the main consequences of the analytical model by means of a numerical experiment.

2. General premises

The model of a point-vortex dynamics on the β-plane, developed in Korotaev (1980*a*, *b*, 1988), is based on some assumptions briefly discussed below.

Let a point vortex of intensity Γ_0 be located at the centre of the coordinate system at the initial moment of time. It follows from the law of absolute vorticity conservation that

$$\nabla^2\psi + \beta y = \Gamma_0\,\delta(x_0)\,\delta(y_0) + \beta y_0 \tag{2.1}$$

at any moment of time, where $\psi = \psi(x, y, t)$ is the stream function, x, y and x_0, y_0 are Eulerian and Lagrangian coordinates, and $\delta(x)$ is the Dirac function.

There are several ways to prove that a cyclonic (anticyclonic) point vortex will move to the north-west (south-west). The point vortex will involve a certain volume of surrounding fluid in its translating movement, as in the case of a moving cylinder with high enough circulation (Batchelor 1967). If the relative vorticity of the fluid involved in the translating movement initially equals zero, fluid particles after meridional displacement will have non-zero relative vorticity. The sign of this vorticity is opposite to Γ_0, according to (2.1). Therefore, if the vortex meridional displacement is large enough, the vortex should be surrounded by a vorticity ring of opposite sign.

Heterogeneity of the relative vorticity distribution inside this ring will be of the order of βR_0, where R_0 is the ring radius. At the same time the mean value of the vorticity may be estimated as $\beta\bar{y}$ if $\bar{y}$ is the meridional displacement of the vortex. Thus, if the vortex travels far enough along the meridian so that $\bar{y} \gg R_0$, it should be surrounded by a ring with approximately constant relative vorticity with sign opposite to Γ_0.

Homogenization of the vorticity inside the ring, which is henceforth called the 'trap zone', will also be promoted by small but finite viscosity. In fact, particles inside the trap zone rotate around the vortex with different angular velocities. After some rotations vorticity gradients will be large enough, and even small viscosity will effectively homogenize the vorticity distribution. According to Korotaev (1980*a*, *b*, 1988) the boundary of the trap zone should be a separatrix of the stream-function field in the moving reference frame.

In the very early stage of its evolution the vortex radiates Rossby waves with a continuous spectrum. These Rossby waves allow the vortex to adjust to a certain quasi-equilibrium state. In the quasi-equilibrium state the vortex radiates only those waves that are quasi-stationary in the frame moving with it.

The meridional component of the vortex propagation velocity is directly related to the radiation of Rossby waves. In fact, the vortex uses up energy in radiating waves, and should decrease in intensity. According to (2.1), this corresponds to its meridional displacement.

Based on the qualitative description presented above, a model of the vortex evolution was developed in Korotaev (1980*a*, *b*, 1988). Comprehensive analysis of the point-vortex model shows that in reality the type of initial vorticity distribution is not very important and all the previous arguments may be applied to the case of continuous vorticity distribution.

3. Mathematical formulation of the problem

The usual equation of the absolute vorticity conservation in terms of the ψ-function is used:

$$\frac{\partial\nabla^2\psi}{\partial t} + \frac{\partial(\psi, \nabla^2\psi)}{\partial(x, y)} + \beta\frac{\partial\psi}{\partial x} = 0, \tag{3.1}$$

where $\partial(f,g)/\partial(x,y)$ is the Jacobian. Let us change to a moving coordinate system with its origin at the eddy centre, where

$$\frac{\partial\psi}{\partial x} = V, \quad \frac{\partial\psi}{\partial y} = -U, \tag{3.2}$$

and U, V are eddy velocity components. Let the stream function at the initial time have the form

$$\psi^0 = -A\,\mathrm{e}^{-(r/l)^2} = -\tfrac{1}{4}\beta l^2 \bar{y}_r\,\mathrm{e}^{-(r/l)^2}, \tag{3.3}$$

where

$$\bar{y}_r = \frac{4A}{\beta l^2} \tag{3.4}$$

is the so-called 'rest latitude' (McWilliams & Flierl 1979).

The model equations are non-dimensionalized by the following characteristic scales for the dependent and independent variables:

$$\left.\begin{aligned} x, y &\sim l, & \bar{y} &\sim \bar{y}_r, \\ t &\sim \bar{y}_r^{\frac{3}{4}}/\beta l^{\frac{7}{4}}, & U &\sim \beta l^{\frac{3}{2}} \bar{y}_r^{\frac{1}{2}}, \\ \psi &\sim \beta l^2 \bar{y}_r, & V &\sim \beta l^{\frac{7}{4}} \bar{y}_r^{\frac{1}{4}}, \end{aligned}\right\} \tag{3.5}$$

where $\bar{y}$ is the eddy displacement along the meridian.

Equation (3.1) in terms of non-dimensional parameters is as follows:

$$\epsilon^7 \frac{\partial\nabla^2\psi}{\partial t} - \epsilon^2 U \frac{\partial\nabla^2\psi}{\partial x} - \epsilon^3 V \frac{\partial\nabla^2\psi}{\partial y} + \frac{\partial(\psi, \nabla^2\psi)}{\partial(x,y)} + \epsilon^4 \frac{\partial\psi}{\partial x} = 0. \tag{3.6}$$

The parameter ϵ which arises in (3.6) is equal to

$$\epsilon = (l/\bar{y}_r)^{\frac{1}{4}}. \tag{3.7}$$

We shall consider this parameter to be small since we are interested in the nonlinear case. This case corresponds to the usual geophysical situation when the eddy translation speed is smaller than the speed of particle inside the eddy. The proposed scaling (3.5) and the small-parameter expression (3.7) follow from Korotaev (1988). As explained in §2, the trap zone boundary is assumed to be the separatrix of the stream-function field in the moving coordinate system (streak function, according to McWilliams *et al.* (1981)):

$$\Psi = \psi + \epsilon^2 U y - \epsilon^3 V x. \tag{3.8}$$

Different types of solution will be constructed inside and outside the trap zone.

The boundary condition on the separatrix follows from continuity of the normal velocity component and pressure. A quasi-stationary regime is assumed, which is why both conditions may be expressed in terms of a stream function with sufficient accuracy:

$$\psi + \epsilon^2 U y - \epsilon^3 V x = 0, \quad \left[\frac{\partial\psi}{\partial n}\right] = 0 \quad \text{at} \quad r = R(\Theta, t, \epsilon), \tag{3.9}$$

where r and Θ are the polar coordinates and $r = R(\Theta, t, \epsilon)$ is the separatrix equation. Square brackets indicate the difference between values just inside and outside the trap zone. An additional restriction is placed on the separatrix form: it is assumed that the separatrix has only one saddle point and that the saddle point has X-coordinate equal

to zero and is located in the upper half-plane for a cyclonic eddy. This restriction may be formulated in the following form:

$$\frac{\partial\psi}{\partial x} = \epsilon^3 V, \quad \frac{\partial\psi}{\partial y} = -\epsilon^2 U \tag{3.10}$$

at $r = R(\frac{1}{2}\pi, t, \epsilon)$.

Conditions (3.2) also should be presented in a non-dimensional form and in the moving reference frame:

$$\frac{\partial\psi}{\partial x} = \epsilon^3 V, \quad \frac{\partial\psi}{\partial y} = -\epsilon^2 U \quad \text{at} \quad x = 0, y = 0. \tag{3.11}$$

The final condition is

$$\psi \to \text{const}\,(t) \quad \text{when} \quad r \to \infty. \tag{3.12}$$

Equation (3.6) with conditions (3.9)–(3.12) yields the final mathematical formulation of the problem. Note that this mathematical formulation does not provide an exact (even in a strict asymptotic sense) solution of the initial value problem for equation (3.6): some fine-scale features of the exact solution are ignored. But the solution that will be constructed is assumed to provide appropriate asymptotics for the eddy structure and velocity when its displacement along the meridian is much more than a radius. The numerical solution of (3.1) will serve to test the basic assumptions presented above.

4. Analytical model of the eddy evolution

The above problem is resolved by a perturbation expansion using an asymptotic series through ϵ^n (Van Dyke 1964). Some additional assumptions are needed because the problem still has a non-unique solution.

The zero-order approximation of the stream function ψ_0 can be found from the equation

$$\frac{\partial(\psi_0, \nabla^2\psi_0)}{\partial(x, y)} = 0. \tag{4.1}$$

Let us choose the solution of (4.1) in the form

$$\nabla^2\psi_0 + \bar{y} = \nabla^2\psi^0 \tag{4.2}$$

inside the trap zone and $\psi_0 = 0$ outside it. ψ^0 is the initial stream-function field (3.3) which has the non-dimensional form

$$\psi^0 = -\tfrac{1}{4}\mathrm{e}^{-r^2}. \tag{4.3}$$

On the boundary of the trap zone ψ_0 satisfies the boundary conditions

$$\psi_0 = \frac{\partial\psi_0}{\partial n} = 0, \tag{4.4}$$

which follow from (3.9).

The problem (4.2), (4.4) with ψ^0 from (4.3) has a unique radially symmetrical solution:

$$\psi_0 = \tfrac{1}{4}\{\bar{y}(1-r^2) - \mathrm{e}^{-r^2} + \bar{y}\ln 1/\bar{y}\}. \tag{4.5}$$

The trap zone is a circle with radius R_0:

$$R_0 = (\ln 1/\bar{y})^{\frac{1}{2}}. \tag{4.6}$$

The first-order approximation satisfies the equation

$$\frac{\partial(\psi_1, \nabla^2\psi_0)}{\partial(x,y)} + \frac{\partial(\psi_0, \nabla^2\psi_1)}{\partial(x,y)} = 0 \tag{4.7a}$$

inside of the trap zone, and the equation

$$\frac{\partial(\psi_1, \nabla^2\psi_1)}{\partial(x,y)} = 0 \tag{4.7b}$$

outside it, and a satisfactory choice of solution is

$$\psi_1 \equiv 0 \tag{4.8}$$

inside as well as outside the trap zone.

The second-order approximation must be considered separately inside and outside the trap zone. Equation (3.6) has the form

$$\frac{\partial(\psi_2, \nabla^2\psi_0)}{\partial(x,y)} + \frac{\partial(\psi_0, \nabla^2\psi_2)}{\partial(x,y)} - U\frac{\partial\nabla^2\psi_0}{\partial x} = 0 \tag{4.9a}$$

inside the trap zone, and

$$\frac{\partial(\psi_2, \nabla^2\psi_2)}{\partial(x,y)} - U\frac{\partial\nabla^2\psi_2}{\partial x} = 0 \tag{4.9b}$$

outside it.

The first of the boundary conditions (3.9) yields

$$\psi_2 = -Uy \quad \text{at} \quad r = R_0. \tag{4.10}$$

The simplest solution of (4.9), (4.10) is $\nabla^2\psi_2 = 0$ and

$$\psi_2 = \begin{cases} -Uy, & r < R_0 \\ \dfrac{\Gamma}{2\pi}\ln r/R_0 - \dfrac{UR_0^2}{r}\sin\Theta, & r > R_0. \end{cases} \tag{4.11}$$

This solution satisfies condition (3.11) for the appropriate expansion order. The unknown Γ (residual vorticity) may be found from condition (3.10):

$$\Gamma = -4\pi R_0 U. \tag{4.12}$$

It is interesting to note that (4.12) corresponds to a more well-known law which arises in the problem of the circulation around a body with a sharp edge (Batchelor 1967).

Finally, the second of the boundary conditions (3.9) gives

$$\left[\frac{\partial\psi_2}{\partial r}\right] + R_2\left[\frac{\partial^2\psi_0}{\partial r^2}\right] = 0 \quad \text{at} \quad r = R_0 \tag{4.13}$$

and using (4.5), (4.6), (4.11), (4.12) we find

$$R_2 = \frac{2U}{\bar{y}\ln(1/\bar{y})}(1 - \sin\Theta). \tag{4.14}$$

Thus, the solution (4.11) with (4.12), (4.14) satisfies all the conditions except (3.12) because of the non-uniformity of the stream-function expansion. Stretched coordinates should be used for the stream-function expansion far away from the trap zone.

Let us introduce stretched coordinates X, Y in such a way that

$$X = \epsilon x, \quad Y = \epsilon y.$$

Assume also that $\psi = \epsilon^2 \tilde{\psi}$. Then we have

$$\epsilon^4 \frac{\partial \nabla^2 \tilde{\psi}}{\partial t} - U \frac{\partial \nabla^2 \tilde{\psi}}{\partial x} - \epsilon V \frac{\partial \nabla^2 \tilde{\psi}}{\partial y} + \epsilon \frac{\partial(\tilde{\psi}, \nabla^2 \tilde{\psi})}{\partial(x, y)} + \frac{\partial \tilde{\psi}}{\partial x} = 0$$

where the Laplacian is also given in new coordinates.

The lowest-order approximation will satisfy the equation

$$-U \frac{\partial \nabla^2 \tilde{\psi}}{\partial X} + \frac{\partial \tilde{\psi}}{\partial X} = 0. \tag{4.15}$$

Equation (4.15) has a solution in the form

$$\nabla^2 \tilde{\psi} - \frac{1}{U} \tilde{\psi} = 0 \tag{4.16}$$

because the eddy moves in undisturbed water.

Bearing in mind the logarithmic asymptotic of (4.11) when $r \to \infty$, the solution of (4.16) is written in the following form:

$$\tilde{\psi} = \frac{\Gamma}{4} \left\{ N_0(\lambda \rho) + \frac{4}{\pi} \sum_{n=0}^{\infty} \frac{J_{2n+1}(\lambda \rho) \cos(2n+1)\Theta}{2n+1} \right\} + \text{const}, \tag{4.17}$$

where $\lambda = (-1/U)^{\frac{1}{2}}$ and $\rho^2 = X^2 + Y^2$; N_0 and J_{2n+1} are the Neuman and Bessel functions.

Equation (4.17) satisfies (3.12) and also the Sommerfeld condition which forbids energy flux from infinity; (4.17) follows from that presented in Flierl (1984) and corresponds to the singular vorticity at the origin of the coordinate system. Equation (4.17) satisfies the matching conditions (Van Dyke 1964) with (4.11). The constant in (4.17) contains $\ln \epsilon$-type terms.

The third-order approximation of the stream function inside the trap zone satisfies the equation

$$\frac{\partial(\psi_3, \nabla^2 \psi_0)}{\partial(x, y)} + \frac{\partial(\psi_0, \nabla^2 \psi_3)}{\partial(x, y)} - V \frac{\partial \nabla^2 \psi_0}{\partial y} = 0. \tag{4.18a}$$

Outside the trap zone but just next to it we have

$$\frac{\partial(\psi_3, \nabla^2 \psi_2)}{\partial(x, y)} + \frac{\partial(\psi_2, \nabla^2 \psi_3)}{\partial(x, y)} - U \frac{\partial \nabla^2 \psi_3}{\partial x} - V \frac{\partial \nabla^2 \psi_2}{\partial y} = 0. \tag{4.18b}$$

The simplest solution

$$\psi_3 = Vx \tag{4.19}$$

inside as well as outside the trap zone and $R_3 = 0$ satisfy (4.18) and all the conditions on the trap-zone boundary.

Bearing in mind that (4.17) has the asymptotic limit

$$\tilde{\psi} \sim \frac{\Gamma}{2\pi} \ln \rho + \frac{\Gamma}{2\pi} \lambda \rho \cos \Theta, \tag{4.20}$$

when $\rho \to 0$, the matching condition gives

$$V = \frac{\Gamma}{2\pi}\lambda = -\frac{2R_0}{(-U)^{\frac{1}{2}}}. \tag{4.21}$$

It is only necessary to obtain the fourth-order approximation inside the trap zone. The equation of this approximation is

$$\frac{\partial(\psi_4, \nabla^2\psi_0)}{\partial(x,y)} + \frac{\partial(\psi_2, \nabla^2\psi_2)}{\partial(x,y)} + \frac{\partial(\psi_0, \nabla^2\psi_4)}{\partial(x,y)} - U\frac{\partial\nabla^2\psi_2}{\partial x} + \frac{\partial\psi_0}{\partial x} = 0. \tag{4.22}$$

The simplest solution of (4.22) is

$$\nabla^2\psi_4 + y - \frac{(\nabla^2\psi_0)_r}{\psi_{0r}}\psi_4 = 0. \tag{4.23}$$

The first of the boundary conditions yields

$$\psi_4 + R_2\frac{\partial\psi_2}{\partial r} + \tfrac{1}{2}R_2^2\frac{\partial^2\psi_0}{\partial r^2} + UR_2\sin\Theta - VR_1\cos\Theta = 0 \tag{4.24}$$

at $r = R_0$.

The solution of (4.23), (4.24) may be presented as the sum of three terms: the first is radially symmetric, the second is proportional to $\sin\Theta$ and the last is proportional to $\cos 2\Theta$. We are particularly interested in the term proportional to $\sin\Theta$ because it describes a dipole, which should transport the eddy.

Let us present the solution of (4.23), (4.24) in the form

$$\psi_4 = \psi_s(r)\sin\Theta + \text{other terms}. \tag{4.25}$$

Then

$$\frac{1}{r}\frac{\mathrm{d}}{\mathrm{d}r}r\frac{\mathrm{d}\psi_s}{\mathrm{d}r} - \frac{1}{r^2}\psi_s - \frac{\dfrac{\mathrm{d}}{\mathrm{d}r}\dfrac{1}{r}\dfrac{\mathrm{d}}{\mathrm{d}r}r\dfrac{\mathrm{d}\psi_0}{\mathrm{d}r}}{\dfrac{\mathrm{d}\psi_0}{\mathrm{d}r}}\psi_s = -r. \tag{4.26}$$

Multiply (4.26) by $r\,\mathrm{d}\psi_0/\mathrm{d}r$ and write it as

$$\frac{\mathrm{d}}{\mathrm{d}r}\left\{r\left[\frac{\mathrm{d}\psi_s}{\mathrm{d}r}\frac{\mathrm{d}\psi_0}{\mathrm{d}r} - \psi_s\frac{\mathrm{d}^2\psi_0}{\mathrm{d}r^2}\right]\right\} = -r^2\frac{\mathrm{d}\psi_0}{\mathrm{d}r}. \tag{4.27}$$

If we integrate both parts of (4.27) from 0 to R_0 using the boundary condition

$$\frac{\mathrm{d}\psi_s}{\mathrm{d}r} = 0 \quad \text{at} \quad r = 0,$$

$$\psi_s = \frac{4U^2}{\bar{y}^2\ln^2(1/\bar{y})}\frac{\mathrm{d}^2\psi_0}{\mathrm{d}r^2} = -\frac{4U^2}{\bar{y}\ln(1/\bar{y})} \quad \text{at} \quad r = R_0$$

the following restrictions arise:

$$R_0\psi_s(R_0)\bar{y}\ln 1/\bar{y} = 2\int_0^{R_0} r\psi_0\,\mathrm{d}r \tag{4.28}$$

or

$$\Gamma U = 2\pi \int_0^{R_0} r\psi_0 \, dr = \iint \psi_0 \, ds = \frac{\pi}{4}[1 - \bar{y}(1 + \ln(1/\bar{y}) + \tfrac{1}{2}\ln^2(1/\bar{y})]. \tag{4.29}$$

This equation together with (4.12) makes it possible to determine the U-component of the eddy velocity. Then using (4.21), the V-component may be found. The result is

$$U = -\frac{1}{4}\left[\frac{1 - \bar{y}(1 + \ln 1/\bar{y} + \frac{1}{2}\ln^2 1/\bar{y})}{\ln^{\frac{1}{2}} 1/\bar{y}}\right]^{\frac{1}{2}}, \tag{4.30}$$

$$V = ((\ln^3 1/\bar{y})[1 - \bar{y}(1 + \ln 1/\bar{y} + \tfrac{1}{2}\ln^2 1/\bar{y})])^{\frac{1}{4}}, \tag{4.31}$$

$$\Gamma = \pi\{(\ln^{\frac{1}{2}} 1/\bar{y})[1 - \bar{y}(1 + \ln 1/\bar{y} + \tfrac{1}{2}\ln^2 1/\bar{y})]\}^{\frac{1}{2}}. \tag{4.32}$$

Formulae (4.30)–(4.32) together with (4.6) and (4.12) provide a full description of the eddy structure and dynamics in the asymptotic case $\epsilon \to 0$. Note that time does not appear implicitly in (4.6), (4.30)–(4.32) or in the expressions for the stream function inside and outside the trap zone. This follows from the quasi-stationarity of the eddy evolution and indicates that the vortex characteristics do not depend on the way in which the vortex achieved its latitude. The function $\bar{y}(t)$ follows from the equation

$$\frac{d\bar{y}}{dt} = V(\bar{y}),$$

which is written in non-dimensional form according to scaling (3.5). This indicates that the quasi-stationary approximation is self-consistent for large enough $\bar{y}$. When $\bar{y}$ tends to zero, $V(\bar{y})$ tends to infinity, and the quasi-stationary approximation does not hold.

It follows from the analytical solution that the kinematics of the eddy is very specific. The eddy itself moves to the west relative to the surrounding fluid and at the same time it is transported to the north by the broad flow induced by a Rossby wave. This appears to be a contradiction but has a simple explanation: the eddy is situated exactly on the same phase of the Rossby wave. Let us mention one more peculiarity of the solution (4.30), (4.31). As a coefficient of the asymptotic expansion, $V(\bar{y})$ is much greater than $U(\bar{y})$. For example $U\ (0.5) \approx 0.05$ but $V\ (0.5) \approx 0.32$. This means that the zonal velocity of the eddy should be much greater than its meridional velocity only when ϵ tends to zero. For small but finite values of ϵ the meridional component may be larger than the zonal one. Such paradoxes may arise when one uses asymptotic series (Van Dyke 1967).

5. Physical sense of the solution

The model described in the previous section has a very simple physical meaning. Equation (4.29) presents the balance between the Zhukovsky–Kutta force (left side) and the Coriolis resultant force arising due to the β-effect. The Zhukovsky–Kutta force acts on the eddy because of the pressure difference on the boundary of the trap zone. This force is exactly the same as in the case of a moving cylinder with circulation (Batchelor 1967).

The Coriolis resultant force arises because particles in the upper and the lower parts of the eddy experience a slightly different Coriolis force action due to the β-effect. It seems that Rossby was the first who noticed this effect (Rossby 1948), which is why this

force can be called a Rossby force. Thus, the U-component of the eddy movement may be found directly from the Zhukovsky–Kutta and Rossby force balance together with (4.12).

The next very clear physical result is related to the eddy energy variation with time. We have that

$$E = \pi \int_0^{R_0} r\left[\frac{\mathrm{d}\psi_0}{\mathrm{d}r}\right]^2 \mathrm{d}r = \frac{\pi}{8}[\tfrac{1}{4}+\tfrac{3}{2}\bar{y}^2 \ln 1/\bar{y}+\tfrac{1}{2}\bar{y}^2 \ln^2(1/\bar{y})+\tfrac{7}{4}\bar{y}^2-2\bar{y}]. \tag{5.1}$$

$$\frac{\mathrm{d}E}{\mathrm{d}t} = \Gamma UV. \tag{5.2}$$

But, on the other hand, if we calculate the energy flux related to Rossby waves radiated by the eddy, namely

$$I = -\int \mathscr{E}(C_{gy}\,\mathrm{d}x - C_{gx}\,\mathrm{d}y),$$

where C_{gx}, C_{gy} are the group velocity components, the expression for the wave energy density $\mathscr{E}$ follows from asymptotics of the stream function (4.17) when ρ tends to infinity. We have

$$\tilde{\psi} \approx \frac{\Gamma}{4}\left(\frac{2}{\pi\lambda\rho}\right)^{\frac{1}{2}} \sin\left(\lambda\rho-\frac{\pi}{4}\right)\left[1+\sum_n (-1)^n \frac{\cos(2n+1)\Theta}{2n+1}\right]$$

$$= \begin{cases} 0 & \text{if} \quad x<0 \\ \dfrac{\Gamma}{4}\left(\dfrac{2}{\pi\lambda\rho}\right)^{\frac{1}{2}} \sin\left(\lambda\rho-\dfrac{\pi}{4}\right) & \text{if} \quad x>0. \end{cases}$$

Thus,

$$\mathscr{E} = \frac{\lambda\Gamma^2}{8\pi\rho} \quad \text{if} \quad x>0.$$

Finally it follows that

$$I = \Gamma UV. \tag{5.3}$$

Thus

$$\frac{\mathrm{d}E}{\mathrm{d}t} = I, \tag{5.4}$$

and the decrease in eddy energy is connected with energy radiation by Rossby waves. Another interpretation of (5.4) is that the eddy energy decrease arises from the work done against the wave drag force.

It is possible to calculate the enstrophy balance for the eddy and the wave field, with the result that the eddy enstrophy decrease is much greater than the Rossby wave enstrophy flux. The explanation of this is obvious in principle. Formula (4.6) yields a decrease in the eddy radius with increasing $\bar{y}$. Thus, there should exist a leakage of eddy vorticity, and a vorticity filament should form along one of the separatrix branches and simultaneously provide the enstrophy balance.

The clear physical sense of the eddy dynamics reflects meridional momentum and energy equations of lower order. In fact all three expressions (4.30)–(4.32) may be deduced directly from momentum projection and energy equations based on the zero-order stream-function approximation inside the trap zone, equation (4.6) for the trap-zone radius, equation (4.12) for residual vorticity, and expression (5.3) for the Rossby wave energy flux as in Korotaev (1980). This is usual when high-order restrictions like (4.28) reflect much lower-order conservation laws. The model is robust

in this sense, and most high-order peculiarities depend on the fact that a vortex carries fluid to the north, conserving absolute vorticity.

6. Numerical experiments

The numerical solution of (3.1) is obtained using a pseudo-spectral model (Orszag 1971) with $N = 128$ spatial quadrature points in each horizontal direction. The domain is square of width 2π, and the flow is periodic on this interval. Thus, the model wavenumber grid has unit spacing and a maximum modulus K_{max} slightly less than $\frac{1}{2}N = 64$. Three values of β were chosen, $\beta = 0.5, 1.0, 10^{\frac{1}{2}}$. To avoid strong oscillations in the relative vorticity fields at the smallest grid scales, hyperviscosity with $\nu = 10^{-7}$ was used as a damping in (3.1).

The initial field for $\psi(x, y)$ was constructed using (3.3) with $A = -1$ and $l = 10^{-\frac{1}{2}}$. This gives more than 12 grid points for the vortex diameter at the initial moment of time.

As was mentioned above, periodic boundary conditions are used. This permits us to exclude the interaction of the vortex with lateral boundaries, but then the problem of vortex self-interaction arises. This problem will produce differences between the numerical and analytical vortices, especially after they have travelled a distance of order of the size of the domain.

As we have chosen the initial amplitude of the vortex in (3.3) with $A = -1$ and $l = 0.1^{\frac{1}{2}}$, from (3.4) we have $\bar{y}_r = -40/\beta$, which for $\beta = 0.5, 1.0$, and $10^{\frac{1}{2}}$, is equal respectively to -80, -40, and -12.65. As noted above, the vortex may only just be considered isolated if its distance from the initial position is more than 2π. But if $\bar{y} = 2\pi$, then $\bar{y}/\bar{y}_r = 0.08$ and 0.15 for $\beta = 0.5$ and 1.0, respectively. Consequently for small enough values of β and $N = 128$ it is possible to obtain an analytical solution only for small $\bar{y}/\bar{y}_r$, which is why most attention will be paid here to the case $\beta = 10^{\frac{1}{2}}$. In this case we may anticipate coincidence of the theory and the experiment up to $\bar{y}/\bar{y}_r = 0.5$, but another problem arises. The parameter ϵ in (3.7) for this value of β is equal to 0.4 and so may hardly be assumed small.

For $\epsilon = 0.4$ an artificial paradox arises. As discussed at the end of §4, the meridional component of the velocity should be about 2.5 times higher than the zonal one. The same result was obtained in the experiment by McWilliams & Flierl (1979) for example. The theory presented in §4, predicts that $-V/U < 1$ should occur for much smaller values of ϵ. Of course, the problem of the applicability of an asymptotic theory arises for such a big value of ϵ. Taking into account the discussion in §5 on the robust properties of the model, we hope that the asymptotic expansion presented in §3, will work even for such a large value of ϵ. Because of the great number of possible uncertainties in the analytical and numerical solutions, we will try to discuss the method of comparison in detail. We hope that such an approach will guarantee reproducibility of the results for other investigators.

7. The structure of the vortex

The theory presented in §3 predicts some specific features of the eddy structure which may be tested using numerical results. Based on the theory the main features of the eddy structure are: approximately radially symmetric stream function and vorticity distribution, a positive-vorticity ring inside the trap zone not only at the very beginning of the eddy evolution, the separatrix of the streak function as a boundary of the trap zone, and a saddle point on the separatrix just to the south of the eddy centre.

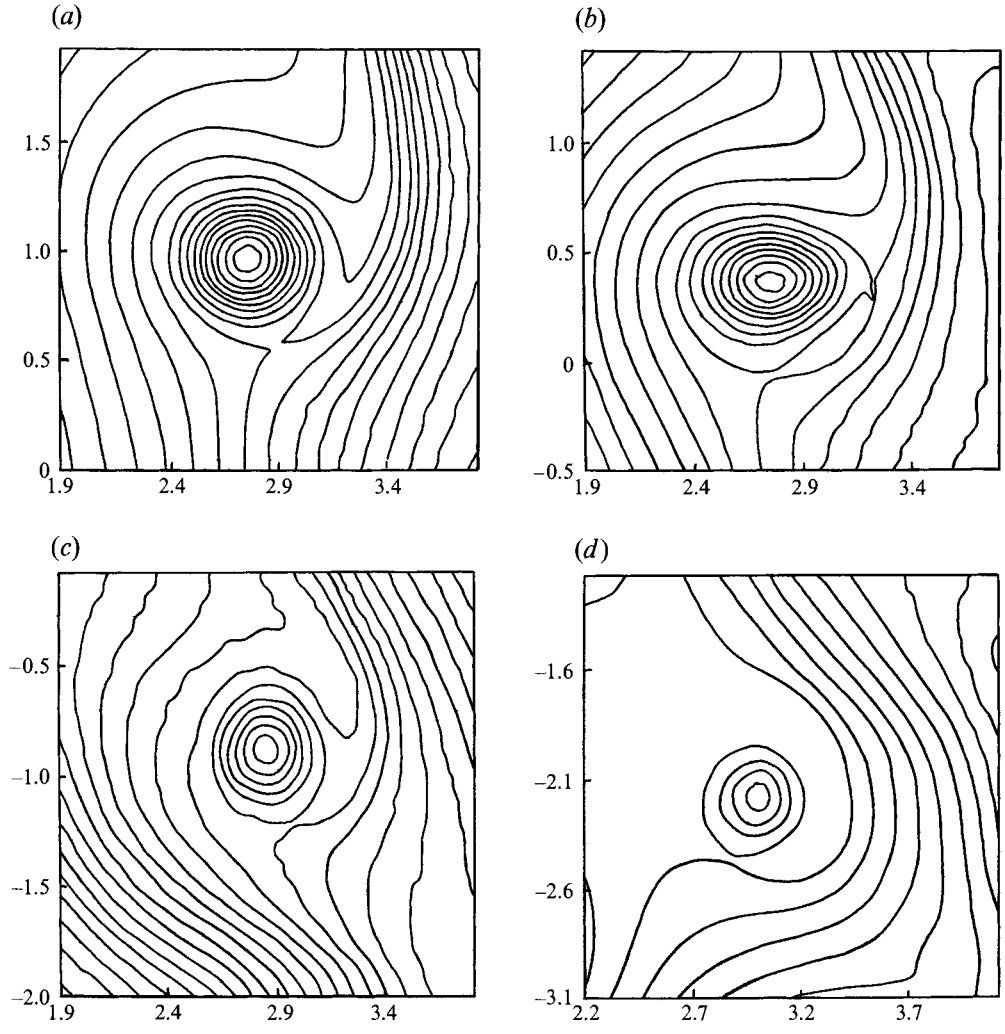

FIGURE 1. Evolution of the streak function with the motion of a vortex on a β-plane. Times shown are: (*a*) $t = 7$; (*b*) $t = 9$; (*c*) $t = 12$; (*d*) $t = 17$. Contour interval 0.05.

We begin the analysis presented here by considering the set of streak functions $\Psi = \psi + Uy - Vx$ for different time moments, where U and V are velocity components determined from the trajectory of the centre of the vortex (figure 1*a–d*). This figure shows a typical picture of the flow near the separatrix, i.e. the position of the saddle point is almost south of the centre of the vortex in spite of the fact that the V-component of the velocity is greater than the U-component. This shows that the vortex moves, relative to the surrounding fluid, almost exactly to the west, in good agreement with the analytical model. Twice during the experiment we observed the appearance of the second saddle point: once at $t = 9$ (figure 1*b*) and again in the final stage of the experiment. The second saddle point was observed to the east of the centre of the vortex in both cases. We shall discuss the first case below. The second one occurs when the influence of the exhausted vortex filament is so strong that it would be wrong to consider the vortex as an isolated one.

To compare the distribution of the relative vorticity inside the trap zone, meridional sections from the numerical experiment and from the theory are presented as a function

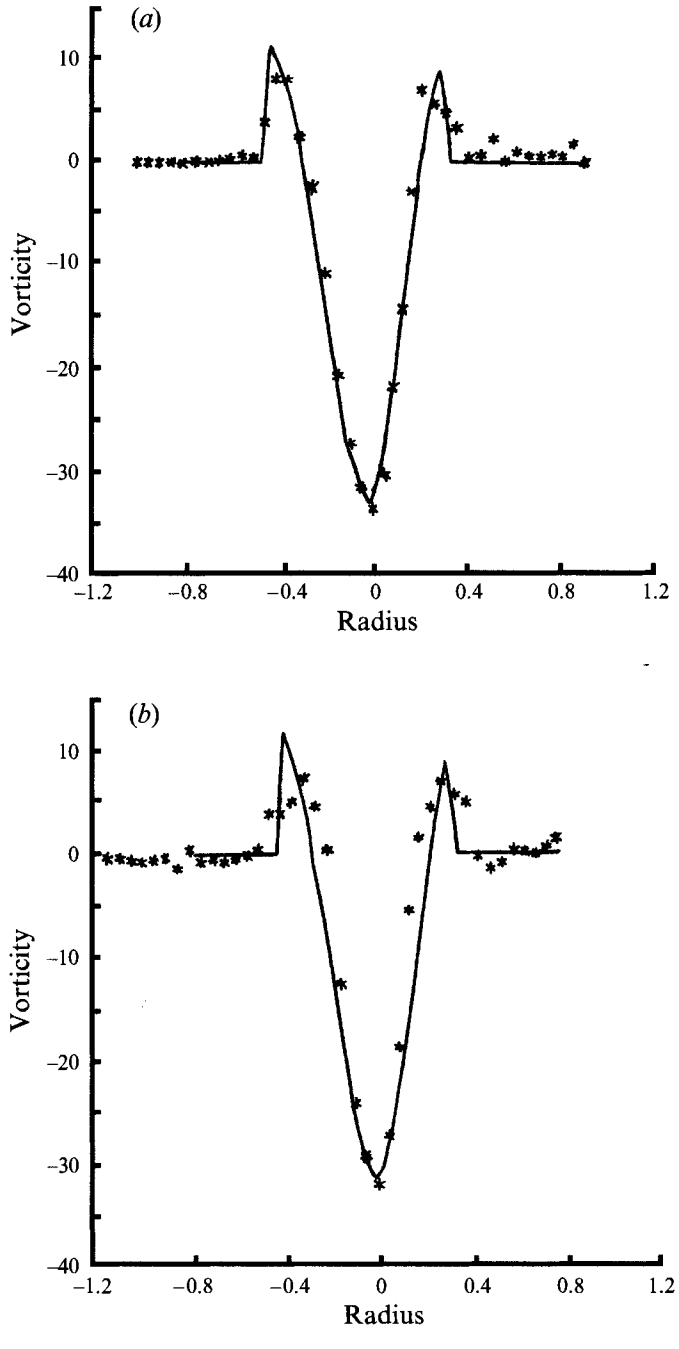

FIGURE 2(*a*, *b*). For caption see facing page.

of radius at $t = 7, 9, 12, 17$ (figure 2). There is good agreement between theory and numerical experiment in the negative-vorticity core. At all times, the negative-vorticity core is surrounded by a positive-vorticity ring. This is of course the consequence of absolute vorticity conservation.

The agreement between theory and numerical experiment in the positive-vorticity ring is expected for initial periods ($t = 7, 9$). The discrepancy between them at $t = 12$

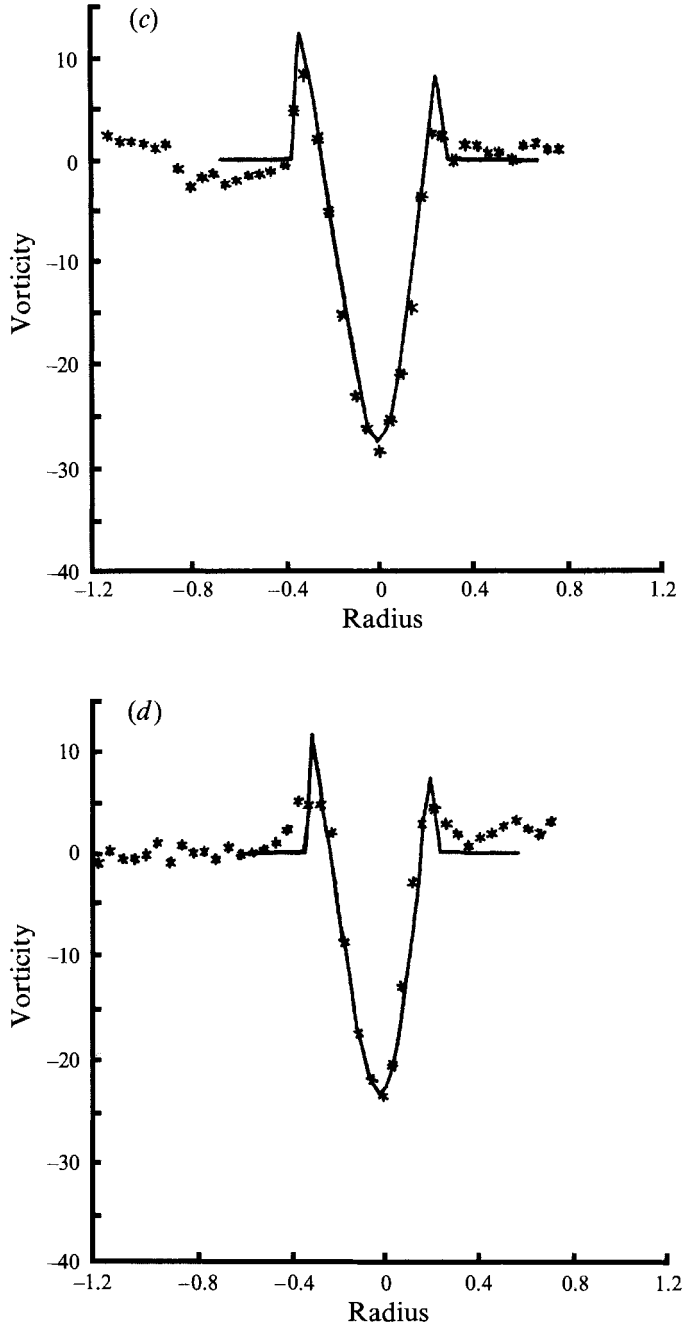

FIGURE 2. Meridional sections of relative vorticity through the centre of the vortex. Experimental values (*) versus theory (solid line). Times shown are: (*a*) $t = 7$; (*b*) $t = 9$; (*c*) $t = 12$; (*d*) $t = 17$.

is caused by non-stationarity in the vorticity field. In addition, diffusion of the relative vorticity is obvious at $t = 17$. The most probable source of diffusion intensification is chaotic fluid particle movement near the separatrix. Outside the theoretically predicted trap-zone boundary the relative vorticity from the numerical experiment tends to zero.

The azimuthally averaged relative vorticity (figure 3) confirms the deductions

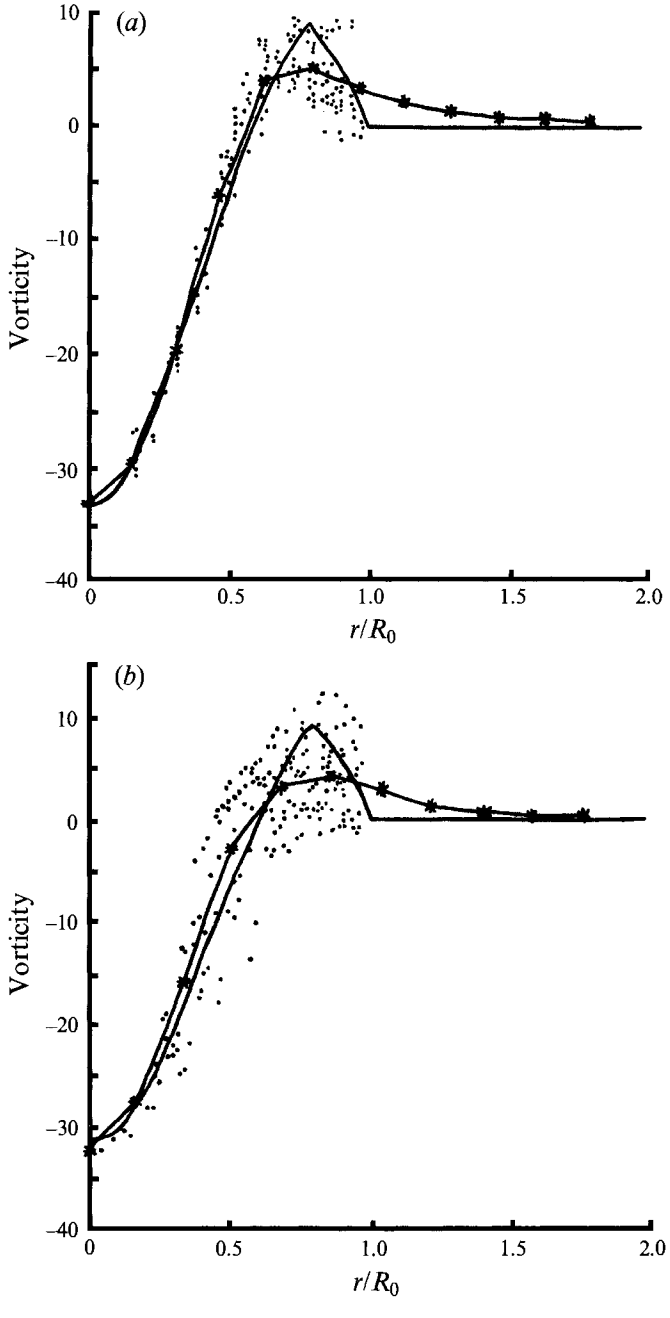

FIGURE 3(a, b). For caption see facing page.

presented above about the existence of a positive-vorticity ring and the decrease of vorticity outside the trap zone. This decrease is not so fast in the numerical experiment as in the analytical theory because of the input of the vortex sheet. Vorticity diffusion is also presented in figure 3 at $t = 17$. All these observations confirm the assumption about the existence of the trap zone inside the separatrix and the zero-relative-vorticity approximation outside it.

The horizontal structure of the relative-vorticity distribution and the separatrix

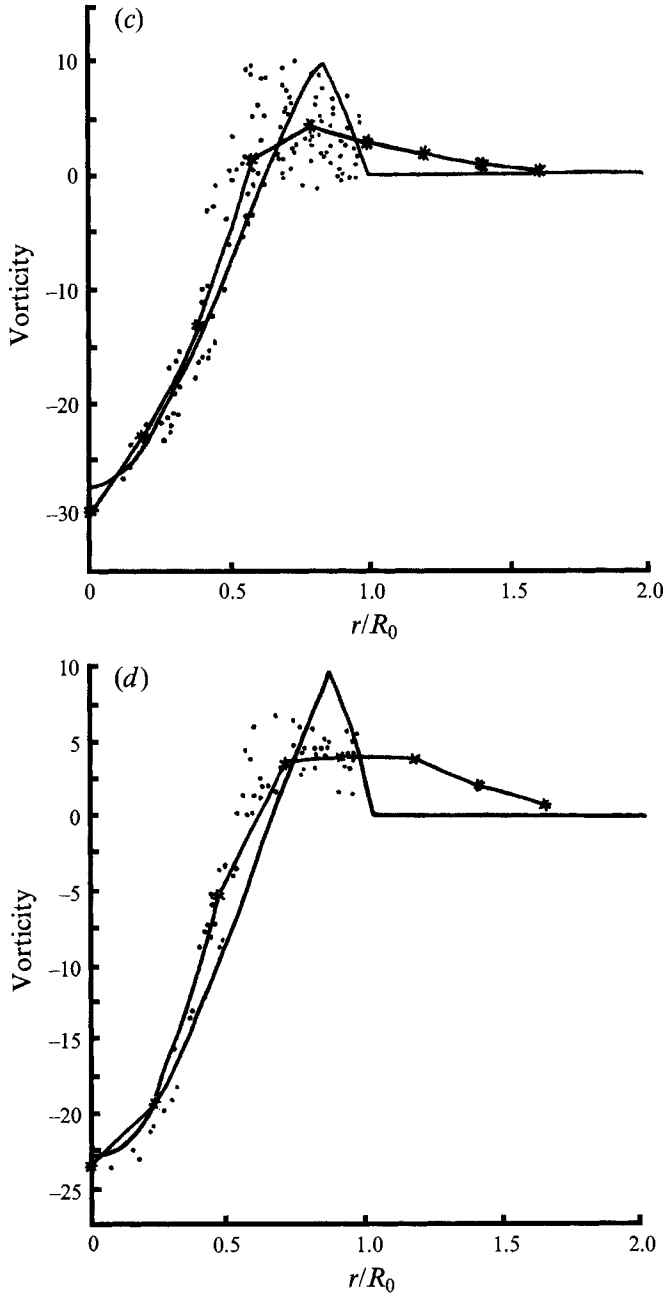

FIGURE 3. Experimental angle-averaged relative vorticity as a function of radius (asterisks connected by the solid line), the theoretical result (solid line), and the experimental values of relative vorticity inside the trap zone (small dots). Times shown are: (*a*) $t = 7$; (*b*) $t = 9$; (*c*) $t = 12$; (*d*) $t = 17$.

position are presented on figure 4. The negative-vorticity core and the ring of positive vorticity inside the trap zone are seen on this figure. The ring of positive vorticity is not homogeneous as suggested by the theory but contains a set of local maxima. Usually two maxima are observed as at $t = 9$ and 12. The most probable reason for maxima formation is a low rotation velocity near the separatrix. When the rotation velocity is

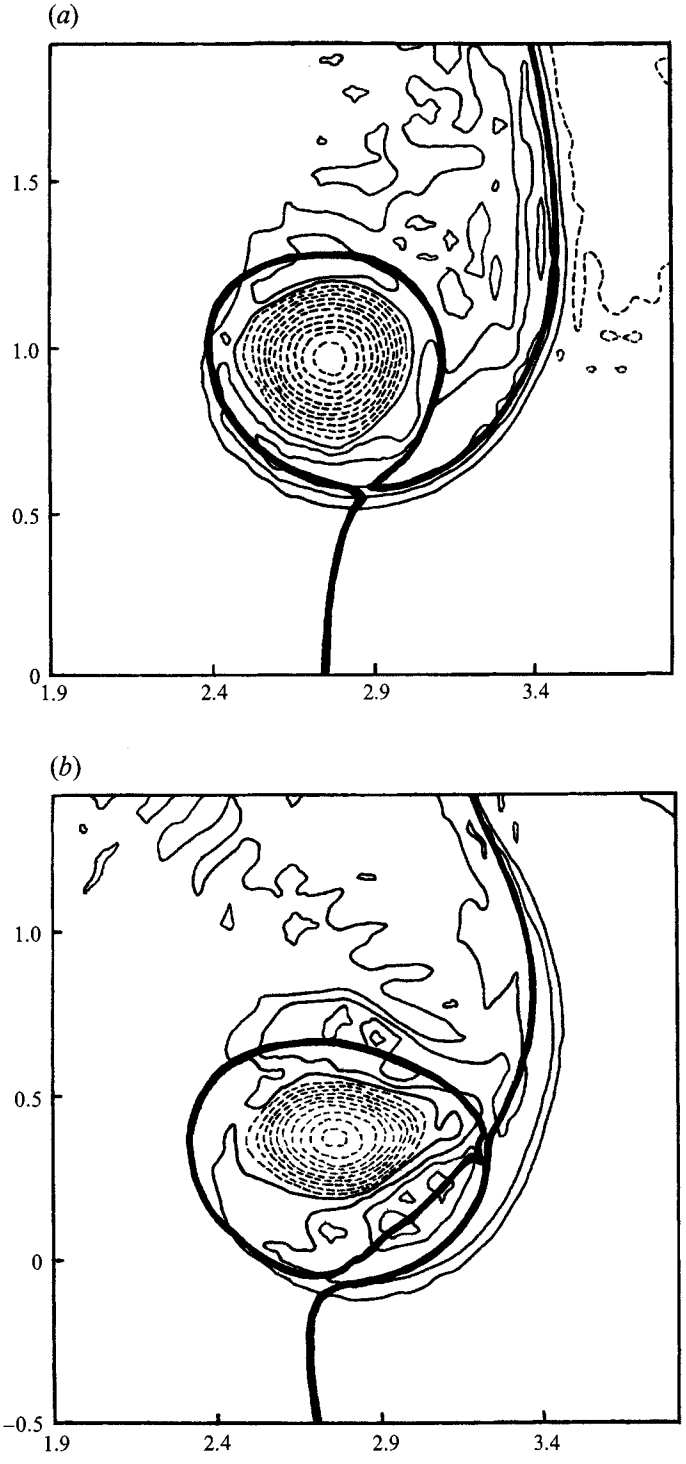

FIGURE 4(*a*, *b*). For caption see facing page.

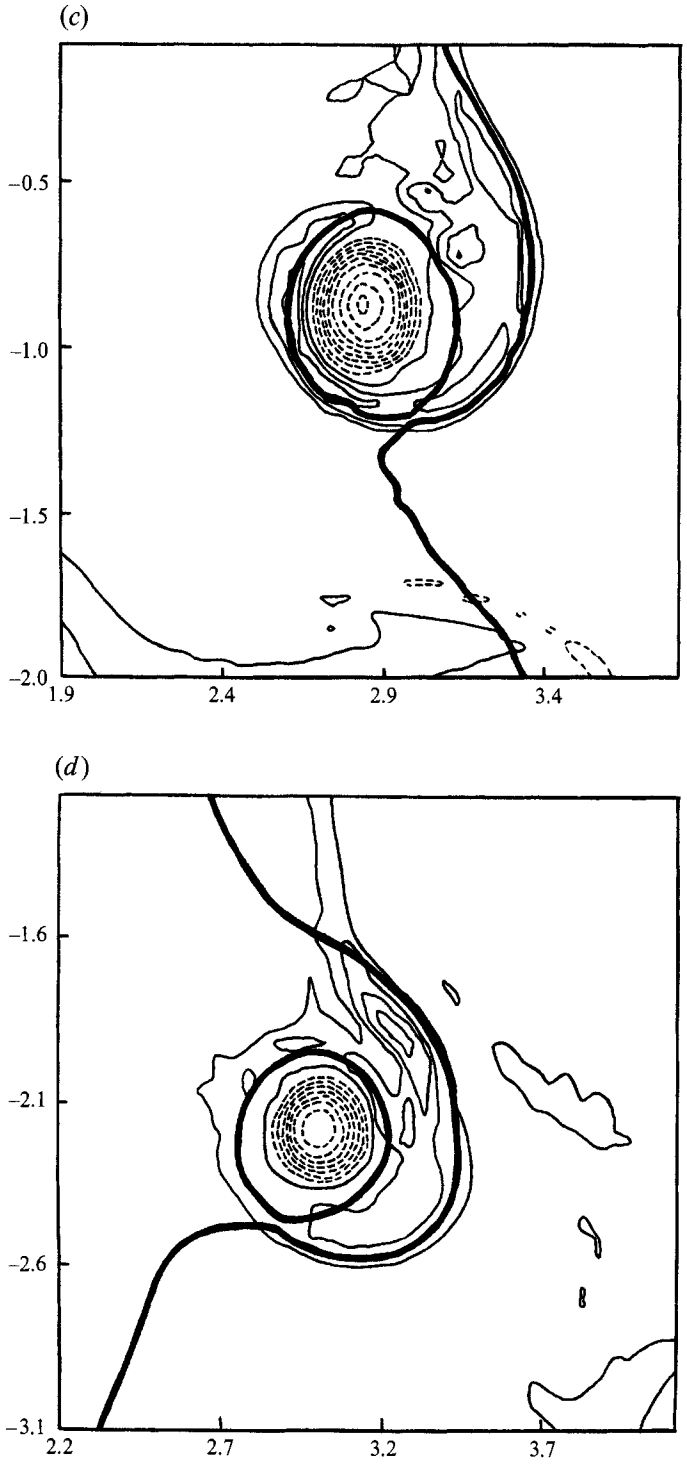

FIGURE 4. Evolution of the relative vorticity with the motion of the vortex; the times shown are the same as in figure 1. Negative values – dashed isolines, positive values – solid isolines. Contour interval 3. The location of separatrix is also shown.

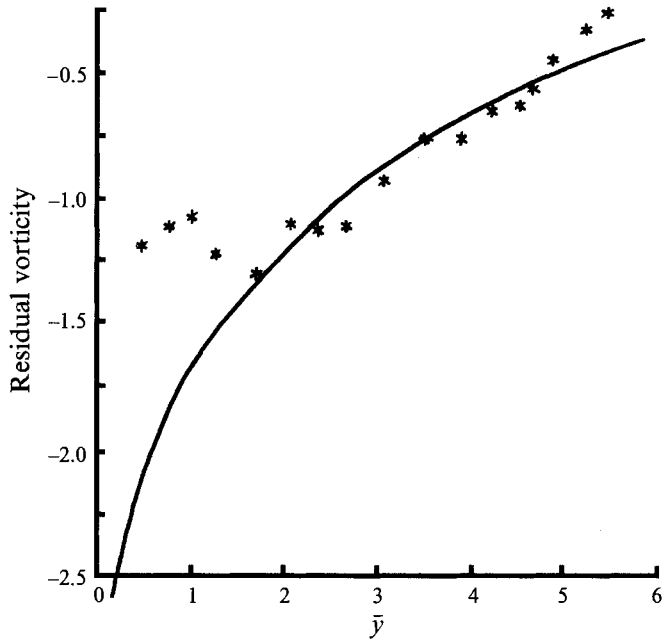

FIGURE 5. Theoretical residual vorticity as a function of $\bar{y}$ (solid line) and experimental values (*) calculated from (7.1) for $t = 1, 2, \ldots, 17$.

close to zero the process of vorticity homogenization is blocked. Non-homogeneity of positive-vorticity distribution inside the trap zone influences the negative-vorticity distribution in the eddy core and produces anisotropy at some time moments such as at $t = 9$ in figure 4.

Positive vorticity maxima compensate the positive vorticity deficit which is seen on the meridional sections on figure 2, at $t = 12$. To illustrate this the residual vorticity was calculated by integration over the trap zone. The residual vorticity is determined here as

$$\left.\begin{aligned} \Gamma(\bar{y}) = \iint_{|\boldsymbol{r}-\boldsymbol{r}_c| \leqslant R_0} \omega(x, y, \bar{y})\, \mathrm{d}x\, \mathrm{d}y, \end{aligned}\right\} \tag{7.1}$$

where $\omega(x, y, \bar{y}) = \nabla^2\psi$, $\boldsymbol{r}_c$ is the radius vector of the eddy centre and $R_0 = l(\ln|\bar{y}_r/\bar{y}|)^{\frac{1}{2}}$ according to (4.6). We prefer to use the y-coordinate of the vortex centre, $\bar{y}$, instead of time, as it is predicted by the analytical theory. The coordinate $\bar{y}$ is determined from the numerical experiment. Figure 5 presents the residual vorticity dependence in terms of $\bar{y}$ according to (7.1) and from the theory (expression (4.32)). The asterisks on figure 5 correspond to $t = 1, 2, \ldots$. The agreement between the theory and the experiment after $t \geqslant 6$ is quite good, showing that in spite of inhomogeneity, the averaged value of the positive vorticity inside the trap zone is very close to the analytical solution.

Another characteristic of the vortex structure which may be tested from the numerical experiment is the trap-zone radius. A reasonable choice for the trap-zone radius is the distance from the vortex centre to the separatrix saddle point. The theoretical value R_0 as a function of $\bar{y}$ is plotted together with R_s, the distance between the centre of the vortex and the saddle point of the separatrix, on figure 6. The value of R_g, the distance between the centre of the vortex and the maximum value of $\mathrm{d}\omega/\mathrm{d}y$ along the meridional section in the southern part of vortex, is also shown on the figure. Figure 6 shows quantitative agreement among all curves and confirms that the

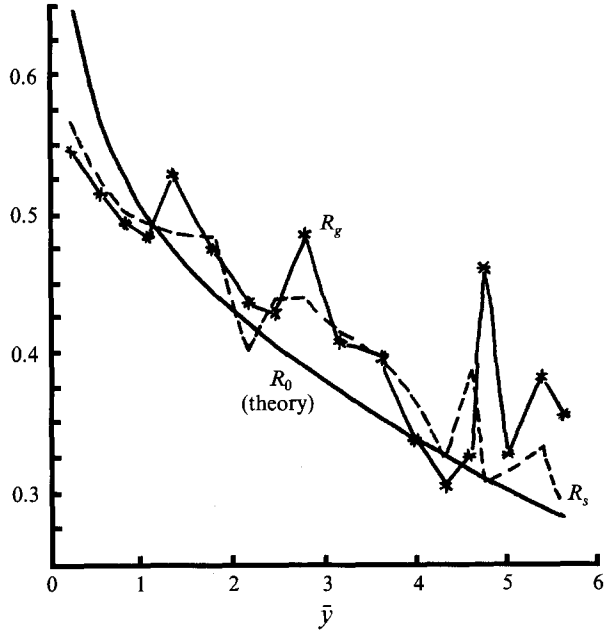

FIGURE 6. Theoretical radius of the trap zone R_0 (solid line) compared to estimates of vortex radius from the experiment: R_g (asterisks connected by solid line) and R_s (dashed line) for $t = 1, 2, \ldots, 17$.

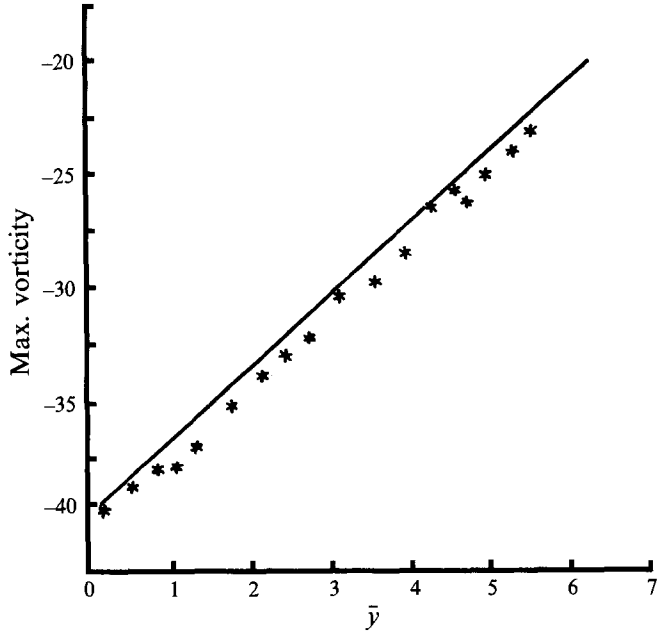

FIGURE 7. Extremum values of the relative vorticity as a function of the drift of the vortex, $\bar{y}$, from its initial location for $t = 1, 2, \ldots, 17$ (*), together with the theoretical result (solid line).

boundary of the trap zone is a line of sharp relative-vorticity variations. The cases of strong variations of R_g which are apparent in figure 6 correlate with strong saddle-point displacements from the usual southern position and will be discussed below.

The next plot (figure 7) illustrates the extremum values of the relative-vorticity $\omega_{max}(\bar{y})$ together with the theoretical line. A linear law $\omega_{max}(\bar{y}) = \omega_{max}(0) - \beta\bar{y}$

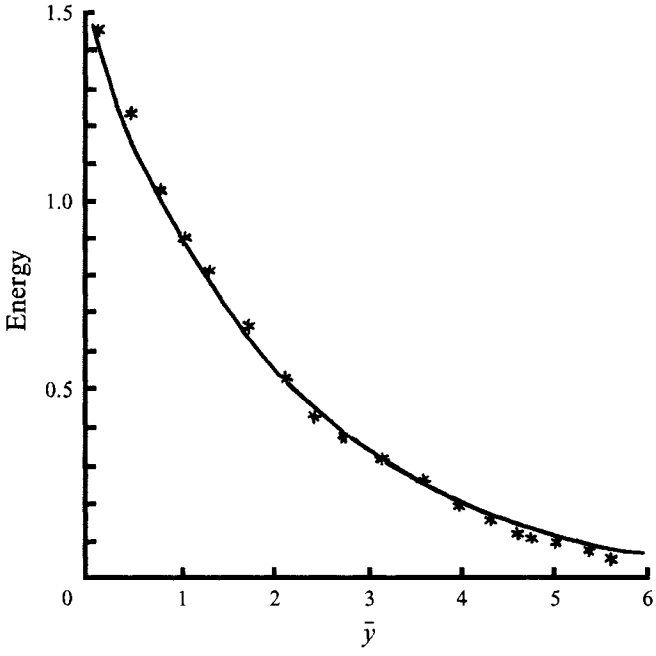

FIGURE 8. Experimental estimates of the kinetic energy of the vortex for $t = 1, 2, \ldots, 17$ (*) and the theoretical curve as functions of $\bar{y}$.

obviously follows from the numerical experiment. This result supports an assumption of §2 that the vortex should involve a certain volume of surrounded fluid in the translating movement. Finally, figure 8 shows the integrated energy of the vortex from the theory and experiment. The theoretical values are calculated according to (5.1) and the experimental ones through the formula

$$E = \frac{1}{2}\int\int(\psi_x^2 + \psi_y^2)\,\mathrm{d}x\,\mathrm{d}y,$$

$$|\boldsymbol{r} - \boldsymbol{r}_c| \leqslant R_0.$$

Agreement between theory and experiment looks perfect. As was mentioned in §6, this is indirect support for Rossby wave radiation. Thus the experimental vortex structure is in general in good agreement with the theory. The main difference between the theoretically predicted vorticity field and the experimental one is in the ring of positive vorticity, where the simulated vorticity field is inhomogeneous and the trap-zone boundary is not so sharp. But apart from this the residual vorticity, the vortex energy, the saddle-point position, and the vortex radius are in good agreement with the theory.

8. The vortex sheet

The most significant feature not reproduced by the theory but appearing in the experiment is vortex sheet formation (figure 4). The source of the vortex sheet is qualitatively obvious. In fact, both the theory and the experiment show a decrease in the trap-zone radius when the vortex moves along the meridian. This is a reason to expect that there should be a leakage of positive relative vorticity from the trap zone into the surrounding fluid. The experiment demonstrates this phenomenon and shows that the leakage of relative vorticity occurs through the saddle point along the

separatrix. Figure 4 shows quasi-one-dimensional vortex sheet formation along the separatrix branch. Some inhomogeneity of the vorticity distribution along the vortex sheet also is observed on figure 4. This inhomogeneity is related to spontaneous leakage of positive-vorticity blobs of the trap zone and this occurs just when the separatrix saddle-point position is shifted from the southern location and sharp variation of R_g is observed.

It is well known (Batchelor 1967) that a one-dimensional vortex sheet is unstable and the phenomenon of quasi-periodic rolling of this structure is observed in the experiment.

9. Kinematic analysis

The velocity components of the vortex movement were used to determine the separatrix position. Here we shall analyse in detail the vortex trajectory and its velocity variation. The experiment under consideration with $\beta = 10^{\frac{1}{2}}$ has the same initial parameters as the experiment by McWilliams & Flierl (1979) and it is convenient to compare vortex trajectories from these two experiments (figure 9). We can see some correspondence between the two experiments. First, we shall concentrate on the dependence of the velocity of the vortex on the displacement of its centre along the meridian.

In the theory presented in § 3 the vortex velocity is the sum of its own velocity relative fluid particles and the translation velocity which translates the vortex as a whole together with surrounding fluid particles. Bearing in mind this idea, the background translation velocity was calculated based on numerical experiment data. It was calculated as an average velocity over the trap zone after removing all the relative vorticity from this zone. Thus, we posed

$$\omega_{tr}(x, y, \bar{y}) = \begin{cases} \omega(x, y, \bar{y}), & |\boldsymbol{r} - \boldsymbol{r}_c| > R_0 \\ 0, & |\boldsymbol{r} - \boldsymbol{r}_c| < R_0. \end{cases}$$

The stream function ψ_{tr} was found from the equation

$$\nabla^2 \psi_{tr} = \omega_{tr},$$

and then the translation velocity components U_{tr}, V_{tr} were determined using averaging over the trap zone. In contradiction with the theory neither component is zero. It is natural to suppose that this is related to the vortex sheet formation and the influence of irregular background vorticity which arises due to the energy and enstrophy lost by the vortex. But in spite of this contradiction we can test the assumption that the vortex velocity is a sum of its own and the translation velocities.

Figure 10 shows U-components of the vortex velocity determined from the trajectory and the vortex's own velocity calculated through the formula (4.30) plus the translation velocity. The theoretical value of the vortex velocity does not differ very much from the experimental one but is systematically higher. Note that the difference between theory and experiment decreases as $\bar{y}$ increases.

Figure 11 presents the V-components of the vortex velocity. The translation velocity and the velocity estimated from the trajectory fit satisfactorily. This confirms the idea of the mechanism of vortex motion as the sum of its own and translation velocities. At the same time the analytical estimation of the V-component is systematically higher than that determined from the experiment (figure 11). But again the difference between the theory and experiment decreases with the growth of $\bar{y}$. So

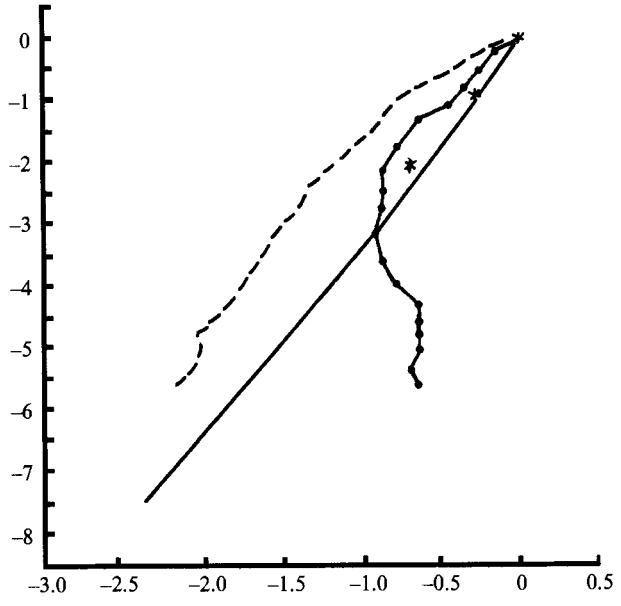

FIGURE 9. The trajectory of the centre of the vortex in physical space (line with dots), the theoretical trajectory (solid line), and the trajectory of the vortex corrected using the x-component of the translation velocity (dashed line) compared to the results by McWilliams & Flierl (1979) (*).

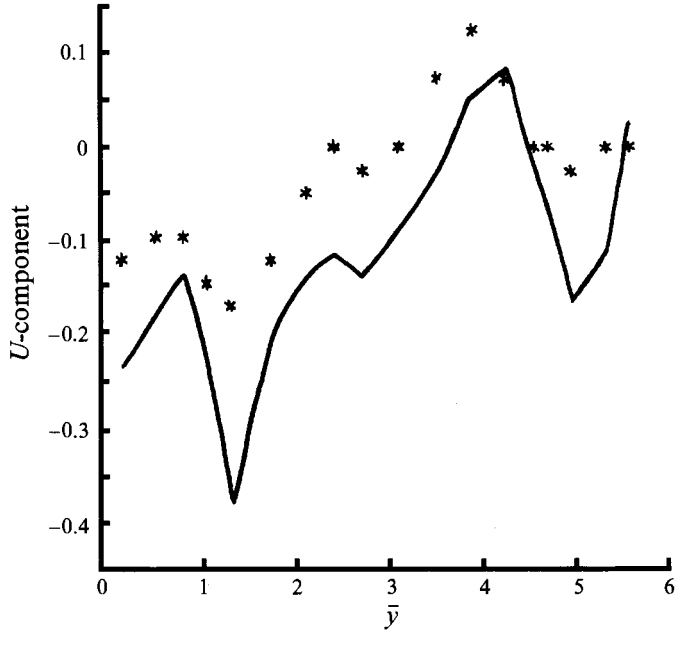

FIGURE 10. Experimental values of the U-component of the velocity of the vortex (*) versus $U_t + U_{tr}$ (solid line), where U_t is the theoretical value and U_{tr} is the U-component of the translation velocity.

it is possible to suppose that the discrepancy between theory and experiment is related to the rather large value of ϵ when $\beta = 10^{\frac{1}{2}}$. The theory works well when the vortex radius is smaller than the length of radiated Rossby waves. This condition is more appropriate for larger $\bar{y}$ when R_0 decreases.

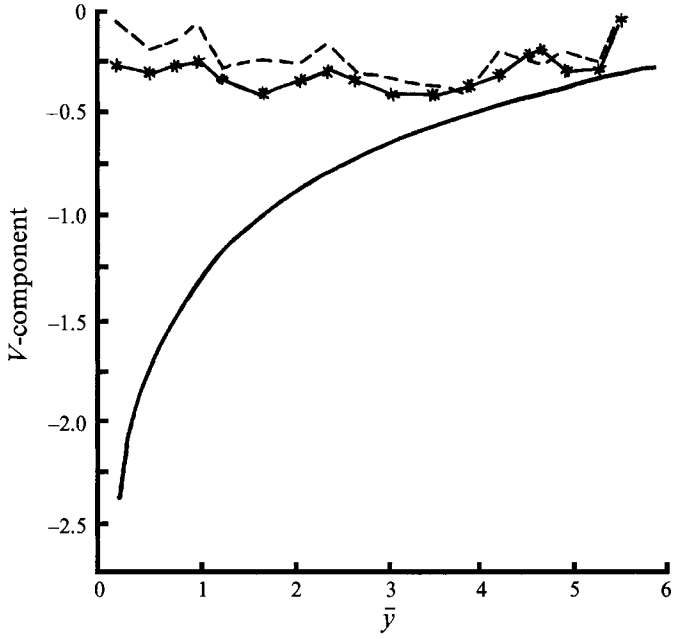

FIGURE 11. Theoretical values of the V-component of the velocity as a function of $\bar{y}$ (solid line), translation velocity (dashed line), and experimental values of the trajectory (solid line with asterisks).

Now let us return to figure 9 where the vortex trajectory from the theory and numerical experiment is presented. The real vortex trajectory from the numerical experiment is quite different from the one predicted by the analytical theory. But if we exclude the U-component from the vortex translation and make an appropriate trajectory correction, the correspondence between the theory and the experiment turns out to be acceptable. At the same time the theoretical vortex displacement exceeds the experimental one because the theoretical approximation does not apply at the initial time.

10. Discussion

The results of analytical and numerical investigations of isolated-vortex kinematics and dynamics confirm our main assumptions. The vortex structure is reproduced from the numerical solution well enough, including the existence of the trap-zone, relative-vorticity distribution, its evolution with the meridional position of the vortex, the separatrix as a boundary of the trap zone and the saddle-point location. Through the estimates of residual vorticity and the zonal component of the vortex propagation velocity, the hypothesis about the relation between relative vorticity, trap-zone radius and the vortex's own velocity (4.12) is confirmed indirectly. The same results confirm the balance between Zhukovsky–Kutta and Rossby forces (4.29). Estimates of the vortex propagation velocity vector from the experiment also support the idea that the vortex translation is the sum of its own velocity directed to the west and the translation velocity induced by the background vorticity.

Good agreement between analytical and numerical solutions is observed after a relaxation period, which corresponds to a displacement of the vortex along the meridian of approximately one-and-a-half or two diameters from the initial position. At the same time the numerical experiment demonstrates some additional charac-

teristics of the vortex which are not prescribed by the analytical solution, namely inhomogeneity of the ring of positive vorticity and vortex sheet formation resulting from vorticity leakage through the saddle point of the separatrix. The non-homogeneity of the ring of positive vorticity does not provide a strong variation of integral characteristics of the vortex, as seen from the residual vorticity and energy estimates. But the vortex sheet obviously influences the vortex kinematics because of the large input to the background vorticity distribution. The irregularity of the background vorticity distribution resulting from an enstrophy cascade to small scales does not give us an opportunity to estimate the exact contribution of the vortex sheet to the translation velocity of the vortex, but it seems probable that the zonal component of the translating velocity may be explained in terms of the influence of the vortex sheet. Unfortunately, the same circumstances also prevent us from testing the Rossby wave radiation phenomenon.

Additional numerical experiments carried out with $\beta = 1$ and 0.5 confirm the conclusions presented above. But we do not present the results of those calculations here because the relation between the domain size and the distance to the rest latitude is so small that the lifetime of the theoretically prescribed regime is too short. However, there is one more point we should like to mention. When we use the scaling prescribed by the analytical theory, characteristics such as the non-dimensional radius of the trap zone, the residual vorticity and the vortex's own velocity components almost coincide for the different values of β mentioned above.

The last remark concerns the functional dependence of the initial vorticity distribution. It is quite evident that the analytical model may easily be applied to a very broad class of initial vorticity distributions.

REFERENCES

ADEM, J. 1956 A series solution for the barotropic vorticity equation and its application in the study of atmospheric vortices. *Tellus* **8**, 364–372.

BATCHELOR, G. K. 1967 *An Introduction to Fluid Dynamics*. Cambridge University Press.

BRETHERTON, F. P. & KARWEIT, M. 1975 Mid-ocean mesoscale modeling. In *Numerical Models of Ocean Circulation* (ed. R. O. Reid, A. R. Robinson & K. Bryan), pp. 237–249. National Academy of Sciences.

CUSHMAN-ROISIN, B., CHASSIGNET, E. P. & TANG, B. 1990 On the westward motion of mesoscale eddies. *J. Phys. Oceanogr.* **20**, 758–768.

FLIERL, G. R. 1984 Rossby wave radiation from a strongly nonlinear warm eddy. *J. Phys. Oceanogr.* **14**, 47–58.

KOROTAEV, G. K. 1980*a* Asymptotical regime of isolated barotropic synoptical eddy dynamics. In *Marine Hydrophysical Investigations N1*, pp. 5–18. Sevastopol: Marine Hydrophys. Inst. (in Russian).

KOROTAEV, G. K. 1980*b* *Structure, dynamics and energetics of synoptical variability of the ocean.* Sevastopol: Marine Hydrophys. Inst. Preprint, 64 pp. (in Russian).

KOROTAEV, G. K. 1988 *Theoretical Modeling of Synoptical Variability of the Ocean.* Kiev: Naukova Dumka (in Russian).

MCWILLIAMS, J. C. & FLIERL, G. R. 1979 On the evolution of isolated, nonlinear vortices. *J. Phys. Oceanogr.* **9**, 1155–1182.

MCWILLIAMS, J. C., FLIERL, G. R., LARICHEV, V. D. & REZNIK, G. M. 1981 Numerical studies of barotropic modons. *Dyn. Atmos. Oceans.* **5**, 219–238.

ORSZAG, S. 1971 Numerical simulation of incompressible flows within simple boundaries. I. Galerkin (spectral) representation. *Stud. Appl. Maths* **50**, 293–328.

ROSSBY, C. G. 1948 On displacements and intensity changes of atmospheric vortices. *J. Mar. Res.* **7**, 175–187.

SHAPIRO, L. J. & OOYAMA, K. V. 1980 Barotropic vortex on a beta plane. *J. Atmos. Sci.* **47**, 170–187.

SMITH, R. K. & ULRICH, W. 1990 An analytical theory of tropical cyclone motion using a barotropic model. *J. Atmos. Sci.* **47**, 1973–1986.

SMITH, R. K., ULRICH, W. & DIETACHMAYER, G. 1990 A numerical study of tropical cyclone motion using a barotropic model. I: The role of vortex asymmetries. *Q.J.R. Met. Soc.* **116**, 337–362.

VAN DYKE, M. 1964 *Perturbation Methods in Fluid Mechanics.* Academic.